Published online 19 April 2021

Nucleic Acids Research, 2021, Vol. 49, No. 12 ***e72***
https://doi.org/10.1093/nar/gkab237

Intermolecular dark resonance energy transfer (DRET): upgrading fluorogenic DNA sensing

Guillaume Barnoin[1], Janah Shaya[1], Ludovic Richert[2], Hoang-Ngoan Le[1], Steve Vincent[1], Vincent Guérineau[3], Yves Mély[2], Benoît Y. Michel[1,*] and Alain Burger[1,*]

[1]Université Côte d'Azur, CNRS, Institut de Chimie de Nice, UMR 7272 – Parc Valrose, 06108 Nice cedex 2, France, [2]Laboratoire de Biophotonique et Pharmacologie, UMR 7213 CNRS, Université de Strasbourg, Faculté de pharmacie, 74 Route du Rhin, 67401 Illkirch, France and [3]Université Paris-Saclay, CNRS, Institut de Chimie des Substances Naturelles, UPR 2301, 91198 Gif-sur-Yvette, France

Received January 27, 2021; Revised March 01, 2021; Editorial Decision March 22, 2021; Accepted April 08, 2021

ABSTRACT

The sensitivity of FRET-based sensing is usually limited by the spectral overlaps of the FRET donor and acceptor, which generate a poor signal-to-noise ratio. To overcome this limitation, a quenched donor presenting a large Stokes shift can be combined with a bright acceptor to perform Dark Resonance Energy Transfer (DRET). The consequent fluorogenic response from the acceptor considerably improves the signal-to-noise ratio. To date, DRET has mainly relied on a donor that is covalently bound to the acceptor. In this context, our aim was to develop the first intermolecular DRET pair for specific sensing of nucleic acid sequences. To this end, we designed DFK, a push–pull probe based on a fluorenyl π-platform that is strongly quenched in water. DFK was incorporated into a series of oligonucleotides and used as a DRET donor with Cy5-labeled complementary sequences. In line with our expectations, excitation of the dark donor in the double-labeled duplex switched on the far-red Cy5 emission and remained free of cross-excitation. The DRET mechanism was supported by time-resolved fluorescence measurements. This concept was then applied with binary probes, which confirmed the distance dependence of DRET as well as its potency in detecting sequences of interest with low background noise.

INTRODUCTION

Since its introduction in the 1950s, Förster resonance energy transfer (FRET) has become an inescapable tool in the life sciences (1–3). Because FRET is distance dependent, it has been used to efficiently probe interactions between biomolecules and a large variety of ligands (4). Due to the predictable distances in nucleic acid (NA) duplexes, studies using FRET-based hybridization probes to detect NAs have been particularly productive (5). Numerous FRET probes have been designed with the aim to specifically detect target sequences (6) in molecular diagnostics (e.g. SNP, genotyping and PCR), screening and interrogation of NAs in living cells (1). Conventional FRET uses bright donor–acceptor pairs based on organic fluorophores. In particular, binary probes were developed that result in FRET when both probes bind to the target and the donor and acceptor come within 10 nm of each other (Figure 1A) (7,8). This reduces the donor emission with a concomitant increase in the red-shifted emission of the acceptor. A common drawback of binary probes is that they generally suffer from cross-excitation of the acceptor at the excitation wavelength of the donor as well as spectral overlap between the donor and acceptor emission (*cross-emission*) (1), because of the small Stokes shifts generally exhibited by FRET dyes (Figure 2A). All these factors contribute to increase the detection limit and also cause false positives. This is particularly critical in homogeneous solutions where the excess of probe cannot be removed, and the emission of the targeted sequence thus corresponds to only a small fraction of the total emission.

One solution to minimize direct excitation of the acceptor is to use a system of three partners, where an intermediate dye serves as a relay to transfer the energy of a donor to an acceptor. This provides a large apparent Stokes shift, but a

*To whom correspondence should be addressed. Tel: +33 4 89 15 01 65; Fax: +33 4 89 15 01 01; Email: alain.burger@univ-cotedazur.fr
Correspondence may also be addressed to Benoît Y. Michel. Email: benoit.michel@univ-cotedazur.fr
Dedicated to the memory of Dr Bang Luu.
Present addresses:
Janah Shaya, College of Medicine and Health Sciences, Khalifa University, Abu Dhabi, P.O. Box 127788, UAE.
Hoang-Ngoan Le, Department of Chemistry and Chemical Engineering, Chemistry and Biochemistry, Chalmers University of Technology, SE-41296 Gothenburg, Sweden.

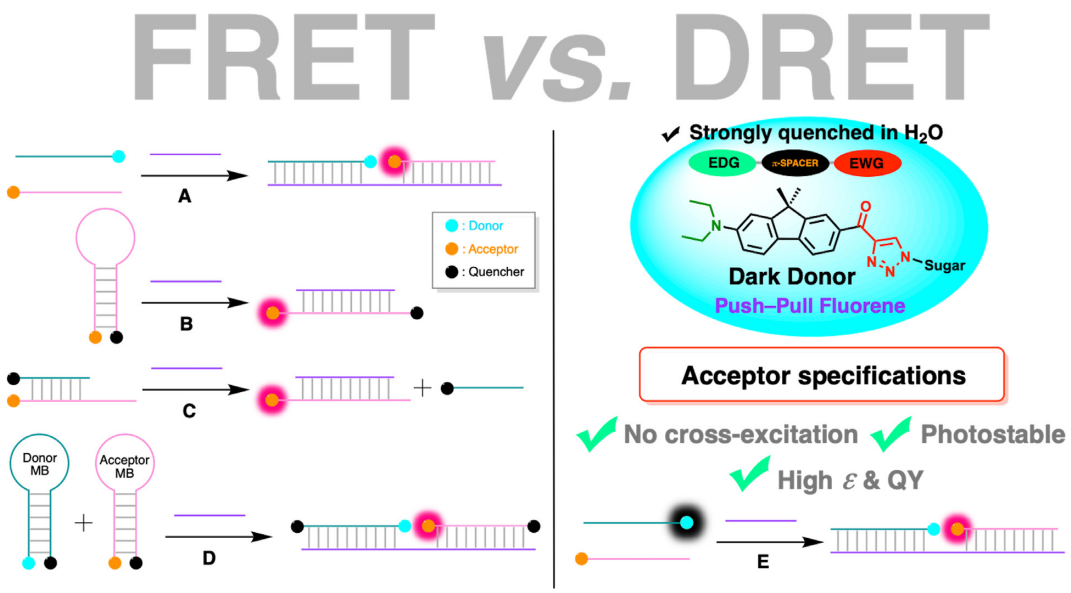

Figure 1. Main strategies implemented for specific sensing of nucleic acids. (*Left*) FRET-based approaches: (**A**) binary probes, (**B**) molecular beacon, (**C**) displacing probe and (**D**) double molecular beacons. (*Right*) Proposed DRET-based approach and (**E**) its application in fluorogenic binary probes.

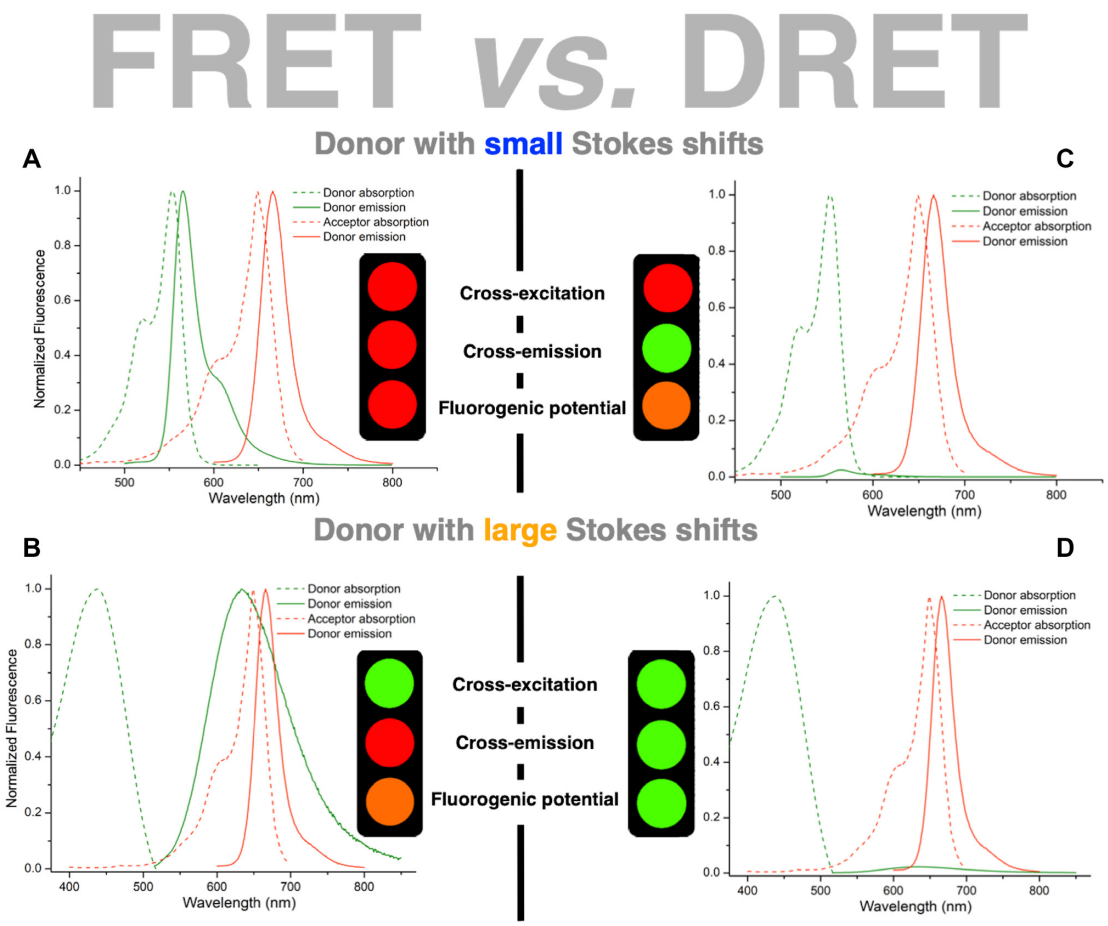

Figure 2. Direct comparison of 'FRET versus DRET' in two different contexts: donor with small (*top*) or large (*bottom*) Stokes shifts, illustrated by representative absorption and emission spectra (compare **A** & **C** and **B** & **D**). The traffic lights indicate the advantages and disadvantages in each case.

less efficient FRET (9). Another effective strategy is to use fluorescence quenchers in place of the acceptor, such as in the popular molecular beacons (MB) introduced by Tyagi and Kramer (Figure 1B). MBs consist of a stem-loop with 5′ and 3′ ends coupled to a fluorophore and a quencher (Q) (10,11). In their closed form, MBs barely fluoresce due to the close proximity of the fluorophore with the quencher, which is essential to reduce the signal-to-noise ratio (S/N). In contrast, binding of the complementary target sequence to the loop opens the stem and removes the dye from its quencher generating a turn-on emission signal. Thus, MBs enable a target-specific, background-free detection with a simple protocol that does not require one to wash out the excess of reagents. This highly efficient turn-on response is especially useful for imaging NAs in cells, where the excess unbound probe cannot be washed out. As an alternative to MB, displacement hybridization probes have also been developed (Figure 1C, 12). In the absence of the target, the donor is quenched by the close proximity of the quencher in the duplex. In the presence of the target, the single strand overhang in the duplex initiates annealing to the target, resulting in an efficient displacement of the quencher strand that switches on the donor emission. It is important to note that MBs or displacement hybridization probes can produce background signals in cells as a result of non-specific interactions with cellular components and/or metabolic degradation (13). To prevent false positives for mRNA imaging in cells, binary probes composed of two MBs were conceived to make the system more specific (Figure 1D, 14,15). Nevertheless, the resulting dual FRET MBs failed to suppress the problems of cross-excitation and cross-emission. Thus, poor S/N remains a critical issue in fluorogenic sensing of NAs, especially in cells where autofluorescence of cellular components can further contaminate the fluorescence signal.

In this context, we hypothesized that binary probes that couple a strongly quenched donor with a large Stokes shift to a bright acceptor might be an attractive solution for fluorogenic sensing of NAs with low cross-excitation and cross-emission. The use of a quenched donor for FRET was recently introduced by Chang *et al.* who built advanced fluorophores with large apparent Stokes shifts by tethering a quenched donor to a bright acceptor (16). This tether led to a highly efficient non-radiative process, called Dark-RET (DRET). The quenching of dark donors in DRET relies mainly on non-radiative intramolecular rotation (17–22). To date, all DRET studies were performed with a donor covalently bound to the acceptor. Our objective was to design, for the first time, a dynamic system with a non-covalently bound DRET pair for fluorogenic sensing of NAs. For the dark donor, we designed the push–pull fluorene DFK (DiethylaminoFluoreneKetotriazolyl) as a nucleobase surrogate with large Stokes shift to minimize cross-emission (Figures 2C, D and 3A, B). As a suitable acceptor, we used the bright Cy5 dye that shows minimal cross-excitation and perfect absorption overlap with DFK emission (Figures 2D and 3B, C). The proof of principle for the intermolecular DRET mechanism was demonstrated by the fluorogenic turn-on of Cy5 emission upon hybridization of DFK-labeled oligodeoxynucleotides with complementary sequences that were Cy5-labeled at either their 5′

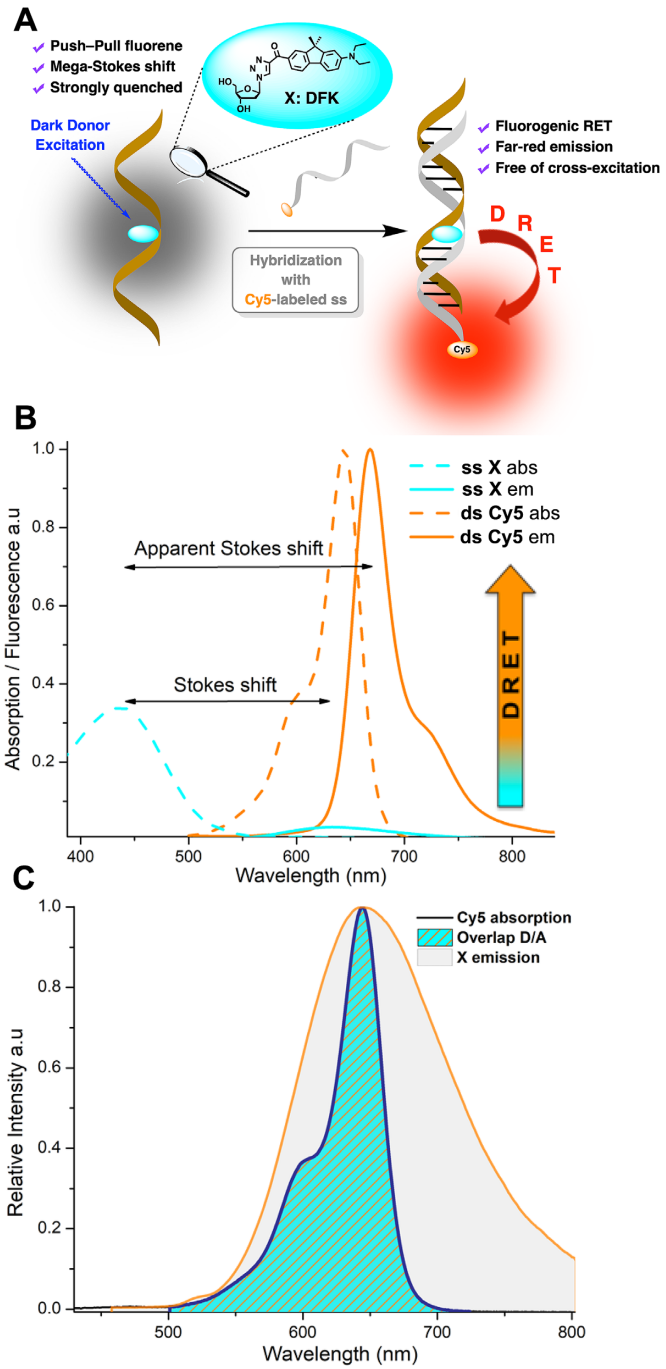

Figure 3. Intermolecular DRET monitored on annealing of a DFK-containing oligonucleotide with its Cy5-labeled complementary sequence. (**A**) Schematic representation of the intermolecular DRET between the push–pull DFK fluorophore used as a quenched donor and Cy5, employed as a bright acceptor. (**B**) DRET-associated photophysics. Absorption (*dashed lines*) and emission (*solid*) spectra of X-labeled single strand (*cyan*) or annealed with its Cy5-labeled complementary sequence (*orange*), highlighting the fluorogenic DRET process coupled with a large apparent Stokes shift. (**C**) Normalized absorption and emission spectra of the respective mono-labeled ds [comp-AGA + TCT-Cy5 (*orange*) and comp-AXA + TCT (*indigo*)] emphasizing the full overlap (*cyan*) of the X–Cy5 RET pair.

or 3′ end. Time-resolved fluorescence measurements confirmed the DRET mechanism. Finally, this intermolecular DRET mechanism was used in the context of binary probes for the recognition of a specific sequence while maintaining low background noise (Figure 1E).

MATERIALS AND METHODS

Synthesis and spectrometry characterization

All reactions involving air- and water-sensitive conditions were performed in oven-dried glassware under argon by using Schlenk techniques employing a dual vacuum/argon manifold system and dry solvents. The synthetic intermediates were initially co-evaporated twice with toluene and dried *in vacuo* before use. All chemical reagents were purchased from commercial sources (Sigma-Aldrich, Acros, Alfa Aesar) and were used as supplied. Anhydrous solvents were obtained according to standard procedures (23). The reactions were monitored simultaneously by liquid chromatography–mass spectrometry (LC–MS) and thin-layer chromatography (TLC, silica gel 60 F254 plates). Compounds were visualized on TLC plates by both UV radiation (254 and 365 nm) and spraying with a staining agent ($KMnO_4$ or ninhydrin) followed by subsequent warming with a heat gun. Column chromatography was performed with flash silica gel (40−63 μm) with the indicated solvent system using gradients of increasing polarity in most cases (24). All NMR spectra (^1H, ^{13}C, ^2D) were recorded on 200 or 400 MHz Bruker Advance Spectrometers. ^1H NMR (200 and 400 MHz), $^{13}C\{^1H\}$NMR (50 and 101 MHz, recorded with complete proton decoupling), and ^{31}P NMR (160 MHz, *proton decoupling*) spectra were obtained with samples dissolved in $CDCl_3$, CD_2Cl_2 or CD_3OD, with the residual solvent signals used as internal references: 7.26 ppm for $CHCl_3$, 5.32 ppm for $CDHCl_2$, and 3.31 ppm for CD_2HOD regarding ^1H NMR experiments, and 77.2 ppm for $CDCl_3$, 53.8 ppm for CD_2Cl_2 and 49.0 ppm for CD_3OD concerning ^{13}C NMR experiments (25). Chemical shifts (δ) are given in ppm to the nearest 0.01 (^1H) or 0.1 ppm (^{13}C and ^{31}P). The coupling constants (J) are given in hertz (Hz). The signals are reported as follows: (s = singlet, d = doublet, t = triplet, m = multiplet, br = broad). Assignments of ^1H and ^{13}C NMR signals were achieved with the help of D/H exchange, COSY, HMQC, HSQC, NOESY and HMBC experiments. LC–MS spectra were recorded using an ion trap Esquire 3000 Plus mass spectrometer equipped with an electrospray ionization (ESI) source in both positive and negative modes. High-resolution mass spectrometry (HRMS) was conducted with a hybrid ion trap−Orbitrap Thermo Scientific™ mass spectrometer (combining quadrupole precursor selection with high-resolution and accurate-mass Orbitrap detection) using ESI techniques.

ODN synthesis, purification and mass characterization

Solid-phase oligonucleotide (ODN) syntheses were performed both on an Expedite 8900 (Applied Biosystem) and H-8 (K&A) DNA synthesizers using the 'trityl off' mode and ultra-mild Pac phosphoramidite chemistry on 1 μmol scale. Reagents and solvents, as well as dT, Ac-dC, Pac-dA and iPr-Pac-dG (or dmf-dG) phosphoramidites were purchased from Link Technologies (LGC) and Chemgenes. Standard DNA assembly 'DMT-off' protocol was employed except for the following modifications: 5-ethylthio-1H-tetrazole (ETT) was used as activating agent; Pac-anhydride was used for capping; a longer coupling time (1200 s) was applied to the fluorenyl phosphoramidite. Labeled ODNs were cleaved from the solid support and deprotected with concentrated aqueous ammonia at room temperature for 12 h. ODNs were analyzed (0.5 ml/min) and purified (2.5 ml/min) by RP-HPLC (HPLC apparatus: Waters™ 600 Controller including Waters™ 996 Photodiode Array Detector and Jasco LC-Net II with ADC) using analytical and semi-preparative C18 columns (Phenomenex™ Clarity® 300 × 4.60 mm and 250 × 10 mm, 5 μm particle size, 100 Å). The following gradient system was used: 100% A – (30 min) → 60% A/40% B – (5 min) → 100% B – (5 min) → 100% A with A = 0.9 TEAB Buffer 100 mM pH 7.8: 0.1 CH_3CN – B = 0.8 CH_3CN: 0.2 TEAB. 100 mM-triethylamine bicarbonate (TEAB) buffer $(Et_3NH)HCO_3$: prepare 0.1 M Et_3N in Milli-Q® water and pass CO_2 into the solution until the pH reaches about 7.8. Store at 4°C. Non-labeled ODNs (used as wild-type sequences) as well as Cy5-labeled ODNs (employed as DRET acceptor sequences) were purchased from Microsynth AG. Dibasic Ammonium Citrate (DAC) (98% capillary GC) and acetonitrile (HPLC grade) were purchased from Sigma-Aldrich. Ultrapure 3-hydroxypicolinic acid (3-HPA) MALDI matrix was obtained from Protea Biosciences. C4 pipette tips (Zip-Tip) were from Millipore. Samples (500 pmol) were diluted to 10 μl of water and were desalted with a C4 pipette Tips (Zip-tip). Zip-tip was activated before use with 2 × 5 μl of water:CH_3CN (50:50) and 2 × 5 μl of DAC (50 mg/ml diluted in water). 10 μl of the ODN solution were loaded on Zip-tip by drawing and expelling ten times. Next, the zip-tip was washed with 3 × 5 μl of DAC (50 mg/ml) and 3 × 5 μl of water. Elution was performed with 1.5 μl of 3-HPA matrix (80 mg/ml, 50:50 CH_3CN:DAC) directly on MALDI plate. MALDI-TOF/TOF-MS analysis: MS spectra were recorded manually in a mass range of 500–6000 Da resulting from 400 laser shots of constant intensity fixed at 6200. Data were collected using 4000 series Explorer (AB Sciex) experiments.

Photophysical characterization (UV–Vis and fluorescence measurements)

All solvents for absorption and fluorescence experiments were of spectroscopic grade. Absorption spectra were recorded at 20°C, on a Cary 100 Bio UV–vis spectrophotometer (Varian/Agilent) using Suprasil® quartz 500 μl cuvettes with 1-cm path length. Stock solutions of DFK or ODNs were prepared using THF or Milli-Q® water. The DFK samples used for spectroscopic measurements contained ≈0.2% (v/v) of solvents of the stock solution. Fluorescence measurements were conducted on a FluoroMax 4.0 spectrofluorometer (Jobin Yvon, Horiba) with a thermostatically controlled cell compartment at 20 ± 0.5°C with slits open to 2 nm and were corrected for Raman scattering, lamp fluctuations and instrumental wavelength-dependent bias. Emission spectra were performed with an absorbance of about 0.05. The excitation wavelength cor-

responds to the absorption maximum of the considered sample.

Quantum yields were corrected according to the variation of the refractive index of the different solvents. They were determined by using 7-(dimethylamino)-fluorene-2-carbaldehyde in MeOH ($\lambda_{Ex} = 385$ nm, $\Phi = 0.46$) as a reference (26), with ±10% mean standard deviation. DFK was analyzed in duplicate at 10 and 2 μM, respectively for UV–Vis and fluorescence measurements. Labeled ODNs were analyzed in duplicate at 2 μM in phosphate-buffered saline pH 7.4 (50 mM sodium phosphate, 150 mM NaCl). In order to ensure reproducibility of hybridization and therefore of measurements, the double-stranded samples were first denatured and then cooled to rt. To estimate the sensitivity of the DRET probe, fluorescence signal amplification was determined according to the following equation $S/N = (F_{hybrid} - F_{buffer})/(F_{ss} - F_{buffer})$ (27).

Additional optical characterization (thermal denaturation and CD spectroscopy)

As previously described, PBS pH 7.4 (50 mM sodium phosphate, 150 mM NaCl) was used as a buffer for each type of experiment. Melting curves were recorded in duplicate by following the temperature-dependence of absorbance changes at 260 nm of the sample (2 μM concentration of each strand). Absorption spectra were recorded in a Peltier-thermostatted cell holder on a Cary 100 Bio UV–Vis spectrophotometer (Varian/Agilent) using Suprasil® quartz cuvettes with 1-cm path length. The temperature range for denaturation measurement was 20–70°C. Speed of heating was 1°C/min. Melting curves were converted into a plot of α versus temperature, where α represents the fraction of single strands in the duplex state. The melting temperatures were extracted from these curves after differentiation as reported (28). Circular dichroism experiments were recorded at 20°C on a Jasco J-810 spectropolarimeter. The wavelength range for CD measurements was 230–320 nm. Spectra were recorded from samples with a concentration of 2 μM for each strand.

Time-resolved fluorescence spectroscopy (TCSPC)

Time-resolved fluorescence measurements were performed using the time-correlated single-photon counting technique (TCSPC). Excitation pulses were generated by a pulse-picked supercontinuum laser (EXR-20, NKT photonics) with superK EXTEND-UV module. Excitation wavelength was set at 430 or 600 nm, with a repetition rate of 10 MHz. The fluorescence emission was collected through a polarizer set at magic angle and a 16-mm band-pass monochromator (H10 Jobin Yvon). The single-photon events were detected with a micro-channel plate photomultiplier (R3809, Hamamatsu) coupled to a pulse pre-amplifier HFAC (Becker-Hickl GmbH) and recorded on a time-correlated single-photon counting board (SPC-130, Becker-Hickl GmbH). The instrumental response function (IRF) was recorded using a polished aluminum reflector, and its full width at half-maximum was ∼50 ps. Experimentally measured fluorescence decays were deconvoluted with the instrumental response function and fitted to retrieve the most probable lifetime distribution using the maximum entropy method (Pulse 5 software) (29). Global fit analysis was performed with the DecayFit software (www.FluorTools.com). In all cases, the χ^2 values were close to 1, indicating an optimal fit. The mean lifetime $<\tau>$ was calculated from the individual fluorescence lifetimes (τ_i) and their relative amplitudes (α_i) according to $<\tau> = \sum \alpha_i \tau_i$.

RET-related parameters

RET parameters (including energy transfer efficiency and rate constant, spectral overlap integral and Förster distance) were calculated according the definitions and Equations (1-5), herein (4). The RET efficiency (E in %) was measured from the donor fluorescence quenching profile according to Equation (1):

$$E = \left(1 - \frac{F_{DA}}{F_D}\right) \times 100 \quad (1)$$

where F_D and F_{DA} are respectively, the relative fluorescence intensities in the absence and presence of the acceptor.

The spectral overlap integral ($J(\lambda)$ in $M^{-1}\cdot cm^{-1}\cdot nm^4$) of the donor emission and the acceptor absorption were determined by using Equation (2):

$$J(\lambda) = \frac{\int_0^\infty F_D(\lambda)\,\varepsilon_A(\lambda)\,\lambda^4 d\lambda}{\int_0^\infty F_D(\lambda)\,d\lambda} \quad (2)$$

where $F_D(\lambda)$ is the fluorescence intensity of the donor in the wavelength range $[\lambda; \lambda + \Delta\lambda]$ and ε_A is the extinction coefficient of the acceptor at λ.

Förster distance (R_0), corresponding to the distance where the RET is 50% efficient, was estimated according to Equations (3 and 4):

$$R_0 = 0.211\sqrt[6]{\left(\kappa^2 n^{-4} Q_D J(\lambda)\right)} \quad (3)$$

$$R_0 = \sqrt[6]{\left(\frac{E}{1-E}\right) r^6} \quad (4)$$

where κ^2 describes the relative orientation in space of the transition dipoles of the donor and acceptor (usually assumed to be equal to 2/3, which is appropriate for dynamic random averaging of the donor and acceptor); n is the refractive index of the medium (1.4 for biomolecules in aqueous solution) and Q_D is the quantum yield of the donor in the absence of acceptor.

r is the donor-to-acceptor distance and it was measured from Equation (5):

$$r = R_0\sqrt[6]{\frac{(1-E)}{E}} \quad (5)$$

RESULTS AND DISCUSSION

Synthesis of DFK and the corresponding amidite

Previous examples of push–pull fluorophores have been designed by conjugating both a dialkylamino group as an electron-donating group (EDG) and a ketotriazolyl moiety as an electron-withdrawing group (EWG) to a π-fluorene

Table 1. Labeled single-stranded ODNs considered in this study with their respective mass and molar extinction coefficient

ODN[a]	Sequence	$[M+H]^+$ observed (calcd)	ε ($M^{-1}\cdot cm^{-1}$)[b]
TXT	5′-CGT TTT **TXT** TTT TGC-3′	4756.2 (4756.2)	137 800
AXA	5′-CGT TTT **AXA** TTT TGC-3′	4775.2 (4774.2)	151 000
CXC	5′-CGT TTT **CXC** TTT TGC-3′	4726.1 (4726.2)	136 600
GXG	5′-CGT TTT **GXG** TTT TGC-3′	4806.6 (4806.2)	142 200
comp-GXG	5′-GCA AAA **GXG** AAA ACG-3′	4877.1 (4878.3)	174 000
comp-AXA	5′-GCA AAA **AXA** AAA ACG-3′	4847.4 (4846.2)	178 200
ret-AXA	5′-GCA AAA **GTG** AXA ACG-3′	4868.7 (4869.3)	174 200
ret-XCG	5′-GCA AAA **GTG** AAA XCG-3′	4869.4 (4869.3)	170 510
TCT-Cy5	5′-Cy5-CGT TTT **TCT** TTT TGC-3′	5150.8 (5150.9)	130 000
comp-GCG-Cy5	5′-Cy5-GCA AAA **GCG** AAA ACG-3′	5281.5 (5273.1)	182 700
comp-TCT-Cy5	5′-Cy5-GCA AAA **TCT** AAA ACG-3′	5223.7 (5223.0)	177 500

[a] ODNs were named according to their central codon.
[b] Molar absorptivity of modified ODNs was calculated from www.atdbio.com/tools/oligo-calculator by considering ε_{260} = 20 000 and 12 500 $M^{-1}\cdot cm^{-1}$ for respectively X and Cy5 (with X = DFK and Cy5 = Cyanine-5).

scaffold (30–32). To introduce this fluorene dye as a base surrogate in NAs, we used our previous convergent approach (30,31) to assemble the naked nucleoside DFK via CuAAC between the 1′-azidodeoxyribose unit and diethylaminofluorenyl ynone (Schemes S1–2, Supplementary Figure S1). The dye could also be introduced into DNA through a linker. Although this solution allows easier access to the labeled ODNs, it was preferred to couple the dye to the 1′-azidodeoxyribose unit in order to make its photophysics more sensitive to the surrounding bases. The photophysical features of this nucleobase mimic were investigated in a wide range of solvents (Supplementary Table S1). DFK absorbed strongly around 410 nm (ε = 42 000 $M^{-1}\cdot cm^{-1}$ in acetonitrile) and displayed moderate solvatochromism ($\Delta\lambda$ = 15 nm, Supplementary Figure S2). In contrast, fluorescence emission exhibited strong solvatofluorochromism along the polarity scale with mega-Stokes shifts exceeding 240 nm (Supplementary Figure S3). According to the Lippert–Mataga model (4), the calculation of the transition dipole moment (14.2 D, Supplementary Figures S4 and S5) confirmed the potent push–pull character of DFK. The quantum yield (QY) of DFK was found to strongly decrease with the proticity of the solvent; thus, the dye shows an exacerbated sensitivity to hydration with a turn-off emission shifted to far-red (Supplementary Table S2, Supplementary Figure S6). The *pK*a of the amino group ($\sim$ 5.8) indicated that the push–pull property is maintained at physiological pH (Supplementary Figure S7). Thus, DFK demonstrates all the prerequisites for being a suitable DRET donor.

Labeled ODNs and their photophysics

DFK was then incorporated in model 15-mer ODNs (Table 1) differing by their contexts (YXY' with Y and Y' = A, T, C or G and X = DFK). The labeled single-stranded sequences (ss-ODNs) were obtained via solid-phase synthesis, purified by RP-HPLC and characterized by UV–vis spectroscopy and MALDI-TOF mass spectrometry (Table 1, Supplementary Figures S8–S16). Each ss-ODN was annealed to its complementary sequence containing a natural base (A, T, C and G) or an abasic site (Ab) at the position opposite X giving 28 duplexes of different compositions (Table 2).

As a first step, the effect of X on the stability and conformation of the duplexes (ds-ODNs) was studied by thermal denaturation and CD spectroscopy (33). With the opposite A, C, G or T, the DFK nucleobase decreased the duplex stability by 3–9°C (Table 2, Supplementary Figure S17), but preserved the canonical B-helical conformation (Supplementary Figure S18). When an abasic site was opposite X, the duplexes were more stable, by 4 to 6°C, than the corresponding wild-type sequences (where G substitutes X). The stability data suggest that the moderate length ($\sim$10 Å) and aromatic character (Supplementary Figure S4) of the fluorescent nucleobase probably enable its correct accommodation into the double helix.

In single strands, the excitation maximum of X is red shifted to 430 nm, independently of the adjacent bases (Table 2, Supplementary Figure S19). Upon hybridization, a further bathochromic shift was observed, reaching 24 nm in the most discriminating case. This result confirmed the propensity of the aromatic fluorophore to stack with the neighboring base pairs (34). Given that the emission is in the red edge of the visible spectrum (649–680 nm for ss-ODNs, 634–659 nm for ds-ODNs), mega-Stokes shifts ranging from 184–247 nm were observed in all cases (Table 2, Supplementary Figures S20–S22). QYs were low and thus, suited for DRET (0.7–6.7%, Table 2). The low QYs and far-red emissions of labeled ODNs were clearly consistent with the results obtained for DFK in highly hydrated media (Supplementary Figures S6 and S23). Hence, the most quenched ODNs displayed the most red-shifted emissions. Altogether, our data suggest that the hydration of X is mainly responsible for its quenching, likely due to the carbonyl group acting as an efficient H-bonding acceptor in ODNs.

Selective excitation and turn-on emission

Proof of concept. The commonly used Cy5 dye was selected as DRET acceptor due to its well-matched properties, such as high brightness (ε = 250,000 $M^{-1}\cdot cm^{-1}$; Φ = 28%) (35), perfect overlap with X donor emission (Figure 3C), and absence of absorption in the 420–480 nm range for Cy5**,** which avoids cross-excitation. To show the proof of principle of intermolecular DRET, X-labeled ss-ODNs were annealed with their complementary sequences labeled with Cy5 at 5′-position through a flexible linker (Table 1, Chart S2). Among all the studied sequences (Table 2), we

Table 2. Spectroscopic properties of **X**-labeled ODNs[a]

ss & ds-ODNs	T_m (°C) Labeled	T_m (°C) Wild type[b]	ΔT_m (°C)	λ_{Abs} (nm)[c]	λ_{Em} (nm)[d]	$\Delta\lambda$[e]	Φ (%)[f]
TXT	-	-	-	429[uv]	654	-	1.8
TXT + ***comp-AAA***	33.7	[42.0]	−8.3	435	654	219	2.2
TXT + ***comp-ATA***	35.6	[42.0]	− 6.4	435	654	219	2.0
TXT + ***comp-ACA***	36.9	[44.7]	− 7.8	441	652	211	2.4
TXT + ***comp-AGA***	36.2	[44.7]	− 8.5	438	654	216	2.1
TXT + ***comp-AAbA***	37.9	32.3	+5.8	439	654	215	2.1
AXA	-	-	-	429	660	231	1.8
AXA + ***comp-TAT***	37.4	[42.0]	− 4.6	444	649	205	2.7
AXA + ***comp-TTT***	36.4	[42.0]	− 5.6	447	648	201	3.1
AXA + ***comp-TCT***	39.6	[44.7]	− 5.1	453	637	184	5.6
AXA + ***comp-TGT***	37.3	[44.7]	− 7.4	444	649	205	3.0
AXA + ***comp-TAbT***	38.0	31.9	+6.1	450	650	200	3.5
CXC	-	-	-	432	649	217	2.7
CXC + ***comp-GAG***	39.6	[47.5]	− 7.9	437	659	222	1.6
CXC + ***comp-GTG***	38.7	[47.5]	− 8.8	437	652	215	1.9
CXC + ***comp-GCG***	41.3	[50.2]	− 8.9	437	655	218	1.4
CXC + ***comp-GGG***	41.3	[50.2]	− 8.9	437	651	214	2.0
CXC + ***comp-GAbG***	43.3	39.3	+4.0	437	652	215	1.5
GXG	-	-	-	434	653	219	2.4
GXG + ***comp-CAC***	44.9	[47.5]	− 2.6	444	641	197	3.7
GXG + ***comp-CTC***	44.9	[47.5]	− 2.6	447	640	193	5.0
GXG + ***comp-CCC***	45.8	[50.2]	− 4.4	448	641	193	4.8
GXG + ***comp-CGC***	45.9	[50.2]	− 4.3	439	653	214	2.4
GXG + ***comp-CAbC***	45.0	40.2	+4.8	446	647	201	3.8
comp-GXG	-	-	-	433	673	240	1.2
comp-GXG + ***CTC***	44.5	[47.5]	− 3.0	443	637	194	5.6
comp-GXG + ***CCC***	45.8	[50.2]	− 4.4	443	640	197	4.7
comp-GXG + ***CAbC***	44.0	39.9	+4.1	443	645	202	3.7
comp-AXA	-	-	-	433	680	247	0.7
comp-AXA + ***TCT***	41.9	[44.7]	− 2.8	448	634	186	6.7
comp-AXA + ***TAbT***	40.2	33.9	+6.3	445	648	203	2.7
ret-XCG	-	-	-	440	666	226	1.7
ret-XCG + ***CAC***	46.7	[47.5]	− 0.8	441	644	203	3.3
ret-AXA	-	-	-	427	671	244	0.7
ret-AXA + ***CAC***	42.4	[47.5]	− 5.1	446	647	201	2.9
comp-GXG + ***CAC***	44.7	[47.5]	− 2.8	440	639	199	2.8

[a] Reported values are the average of two or more independent and reproducible measurements, ±1 nm for wavelengths.
[b] Theoretical T_m value of the corresponding duplex formed from unmodified ODNs (calculated from www.atdbio.com/tools/oligo-calculator); given in square brackets.
[c] Position of the absorption maximum in nm. Excitation wavelength was at the corresponding absorption maximum.
[d] Emission maximum in nm.
[e] For convenience, Stokes shifts are expressed in nm for $\Delta\lambda = \lambda_{Em} - \lambda_{Abs}$ (difference in cm^{-1}).
[f] Fluorescence quantum yields Φ were determined using an excitation at the corresponding absorption maximum of X, ±10% mean standard deviation. 7-(dimethylamino)-fluorene-2-carbaldehyde in MeOH (λ_{Ex} = 385 nm, Φ = 0.46) was used as a reference (26).

selected the X-labeled ds-ODNs with the lowest and highest QYs (CXC + *comp-GCG*: Φ = 1.4% and comp-AXA + *TCT*: Φ = 6.7%). Assuming a 3.4 Å gap per base pair for B-DNA and a random orientation of the donor and acceptor, the distance between X and tethered Cy5, which is known to stack at the end of the duplex (36), should be around ≈ 30 Å (3,37–39). This distance is favorable for RET as the calculated Förster distances, R_0 (distance at which RET efficiency is 50%) were found to be 33 and 46 Å for the darkest and brightest duplexes, respectively (4).

Comparison of the fluorescence spectra of the ds comp-AXA + *TCT* with comp-AXA + *TCT-Cy5* indicated an almost complete disappearance of the X donor emission coupled to a very strong increase in the emission of Cy5 acceptor, which are evident signatures of RET (Figure 4A). Transfer efficiency was determined to be 83%. The strong increase in Cy5 fluorescence is clearly not related to a direct excitation of Cy5, as can been seen from the very low emission of the comp-AGA + *TCT-Cy5* duplex (*black curve*, Figure 4A) and the low increment in fluorescence when the Cy5-labeled complementary strand was added in 10 eq. excess to the duplex comp-AXA + *TCT-Cy5* (green versus magenta spectra, Figure 4A). In comparison with ss comp-AXA, a 100-fold amplification was observed in the emission of Cy5 at 665 nm for the comp-AXA + *TCT-Cy5* duplex. Very similar observations were made for the comparison of the CXC + *comp-GCG-Cy5* duplex with the CXC + *comp-GCG* duplex and the ss CXC oligonucleotide (Figure 4B). Due to a smaller R_0 (33 Å), a lower transfer efficiency of 55% was calculated. An 8-fold increase in the fluorescence signal was observed at the emission maximum of Cy5 (665 nm) after hybridization of CXC to *comp-GCG-Cy5* demonstrating the sequence dependance of the system. Nevertheless, the strong increase in Cy5 was again unrelated to cross-excitation but was caused by RET between X and Cy5. The RET mechanism was further supported by the anisotropy

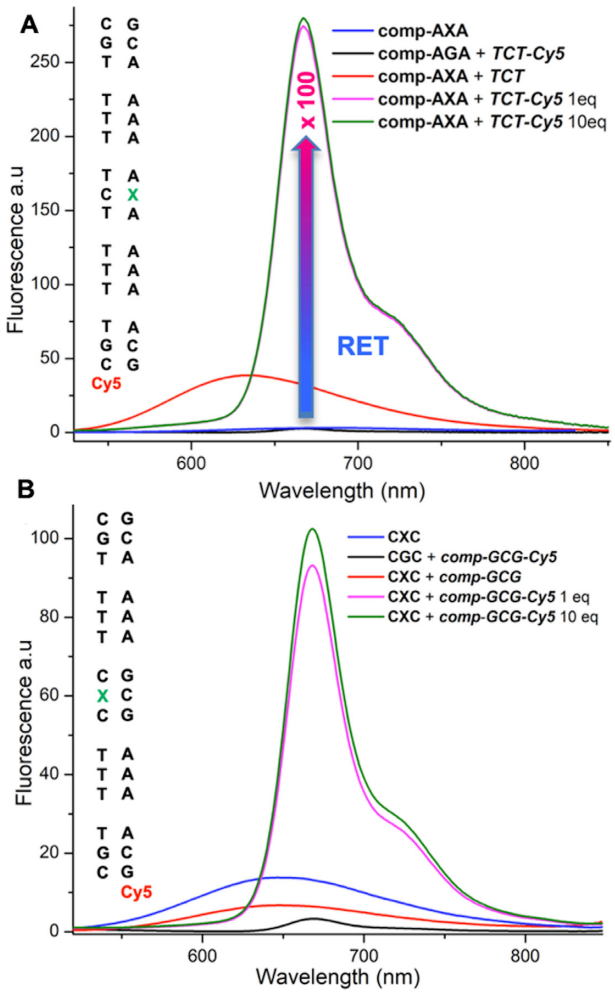

Figure 4. Emission spectra of the (**A**) comp-AXA + *TCT* and (**B**) CXC + *comp-GCG* ds-constructs in presence or absence of Cy5 acceptor on the complementary strands. In A) the RET between X and Cy5 led to a 100-fold increase in the fluorescence signal. Samples were recorded at *2* μm, in pH 7.4 PBS and excitation was performed at the donor absorption maximum.

measurement of the acceptor at 667 nm, showing that excitation through RET at 430 nm leads to strong depolarization ($r \approx 0.04$) as compared to direct excitation at 600 nm ($r = 0.26$) (40). To complete our understanding of this fluorogenic process, time-resolved measurements were also performed.

Time-correlated single photon counting. For the free nucleoside DFK, a monoexponential decay was obtained in THF, with a fluorescence lifetime $\tau_{(THF)} = 2.8$ ns (Supplementary Figure S24). In EtOH, the lifetime decay dropped ($\tau_{(EtOH)} = 0.3$ ns) in agreement with the decrease in QY (Supplementary Table S1). Excitation at the absorption maximum (430 nm) of comp-AXA in its ss-form resulted in a biexponential decay with a major component (94%) at 0.23 ns and a minor component at 0.65 ns (Supplementary Figure S25). The value of 0.23 ns is close to the lifetime of X in EtOH, which is consistent with the known polar surroundings of nucleotides in ss-ODNs. Interestingly, once the

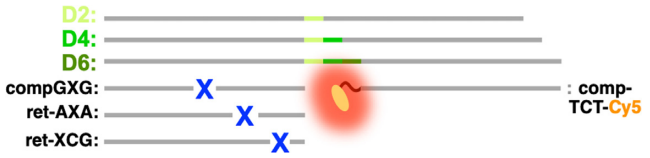

Figure 5. Gapped-junction-based system for distance-dependence DRET investigations: D2, D4 and D6 correspond to the target DNAs with a gap junction of two, four and six nucleotides, respectively. Binary probes labeled with X and Cy5 are complementary to D2, D4 and D6 on both sides of the gapped junction.

duplex is formed with TCT, the fluorescence decay became monoexponential with a lifetime of 0.64 ns (Supplementary Figure S25). This 2.5-fold increase in lifetime is fully consistent with the more apolar environment around X after hybridization.

In the next step, we investigated the time-resolved fluorescence decays of the same duplex, but this time, in presence of Cy5. First, the decay of the acceptor was recorded in the duplex by exciting at 630 nm where only Cy5 absorbs. A monoexponential decay was monitored with a lifetime $\tau_{(Cy5)} = 1.28$ ns at both 675 and 730-nm emission wavelengths (Supplementary Figure S26). Next, the emission decay of comp-AXA + *TCT-Cy5* was measured, by exciting at 430 nm where Cy5 absorption is negligible (Supplementary Figure S27). The emission decay was first recorded at 600 nm (Supplementary Figure S27), where only X emits (Supplementary Figure S28). The fluorescence decay was well fitted with a major (96%) component at 0.12 ± 0.01 ns and a minor one (4%) at 0.69 ± 0.05 ns. This biexponential decay with a minor component – identical to the lifetime of X in duplex in absence of Cy5 – together with a short-lived lifetime is typical of a RET donor (4, 41).

To confirm the RET between X and Cy5, the emission decay of the doubly labeled duplex was monitored at 675 and 730 nm (Supplementary Figure S29) where the emission is largely dominated by Cy5 (Supplementary Figure S28). As Cy5 cannot be directly excited at 430 nm, its excitation ought to predominantly occur through RET from X. Accordingly, the acceptor decay function is expected to be the convolution of the fast decay of X with the natural decay function of Cy5. As a result, the decay function of comp-AXA + *TCT-Cy5* should have a rising component with a time constant equal to the RET lifetime of the donor (42, http://www.becker-hickl.de/pdf/SPC-handbook-6ed-12-web.pdf). In fluorescence decays, rise components, which are commonly associated with excited-state reactions, appear with a negative amplitude and can therefore be easily identified. To demonstrate the presence of this rise component, we first fitted the decay at 675 nm with only positive components. Even when using 3 components, the fits of the fluorescence decay were poor as shown by the high χ^2 value and the non-random distribution of residuals, especially for the first channels of the decay curve (Supplementary Figures S29A and B). Inclusion of a rise component was found to substantially improve the fit and the distribution of residuals (43). An optimal fit was obtained when the rise component was associated with two positive components, one (1.28 ns) being the lifetime of Cy5

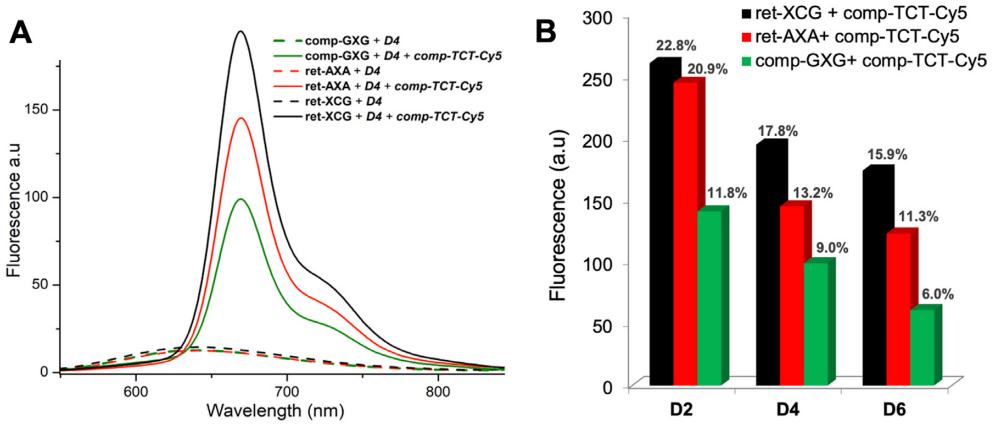

Figure 6. Distance impact on DRET: (**A**) emission spectra displaying distance dependent changes in fluorescence with gaps of two, four and six nucleotides for the D4 system (**B**) Histogram comparing the relative fluorescence intensity of the three considered ternary D2, D4 and D6 systems. Pseudo quantum yields of the DNA constructs undergoing RET were mentioned on the top of their relative bar. Sample concentration was 2 μM in pH 7.4 PBS, and excitation was set at the donor absorption maximum.

(Supplementary Figure S29C). Similar outcomes were observed with an emission at 730 nm (*data not shown*).

To further validate our conclusions and to find the optimal values of fluorescence lifetimes, a global analysis was performed by simultaneously fitting the fluorescence decays of comp-AXA + *TCT-Cy5* recorded at the three wavelengths, by constraining the decay times to be the same for all decays but allowing their amplitudes to vary (4). Using this approach, the best fits were obtained with the following three lifetimes: $\tau_1 = 90$ ps, $\tau_2 = 560$ ps, and $\tau_3 = 1.28$ ns (Supplementary Table S3). The value of the rise component ($\tau_1 = 90$ ps) is fully consistent with the RET-associated short-lived lifetime ($\tau_1 = 120$ ps) of the donor X in the comp-AXA + *TCT-Cy5* duplex (*vide supra*), as expected for RET between X and Cy5. From the RET-associated short-lived lifetime of the donor X ($\tau_1 = 120$ ps) and a Förster distance of 46 Å for the X/Cy5 pair, a RET efficiency of 81% and a distance r of 36 Å was calculated between the two dyes (Equations 1–5). This distance is in accordance with the theoretical 30 Å distance (*vide supra*). Moreover, the RET efficiency determined from lifetime ($E = 81\%$) and steady-state ($E = 83\%$) experiments fully converged, which further confirms the consistency of the data.

Altogether, our data indicate that DRET turns on Cy5 emission with high amplification and is free of cross-excitation (Figure 4).

Application. To demonstrate the potential for intermolecular DRET in DNA sensing, we designed a set of binary probes labeled with X and Cy5, respectively, that are complementary to a long target sequence. The annealing of the binary probes with the target sequence leads to a gap of two, four or six nucleotides (D2, D4 and D6) (Figure 5, Supplementary Figure S30). A gap of at least two nucleotides between the probes is thought to avoid problems related to dipole orientation (44). Moreover, to further vary the distance between X and Cy5 in their ternary complexes with their target sequences, the position of X was changed in the X-labeled probe.

The donor was found to show a similar QY upon hybridization (close to 3%) with the target sequence in the absence of Cy5-labeled probe in all the constructs (Supplementary Figure S31). As a result, R_0 is constant ($R_0 \approx 40$ Å) in all systems and the distance effect in the RET process can be easily deduced from comparison of the spectra. In the ternary complexes, by reducing the distance between the donor and the acceptor – either by shortening the gap D6−>D2 or moving X – a gradual increase in Cy5 fluorescence intensity was observed as expected for RET (Figure 6 & Supplementary Figure S32). The brightest signals were obtained for ret-XCG and ret-AXA in association with D2 + *comp-TCT-Cy5* where the donor-to-acceptor distance is the shortest. If we define the ratio of the number of photons emitted by the acceptor to that absorbed by the donor as a *pseudo* quantum yield, Φ_{ps}, the values of Φ_{ps} (21–23%, Figure 6B) are comparable to the quantum yield of Cy5 ($\Phi = 28\%$) indicating an almost quantitative energy transfer from the donor to the acceptor. For both D4 and D6 systems, a progressive decrease of Φ_{ps} was observed when R_{D-A} increased as well as a strong depolarization of the Cy5 emission, which are consistent with a RET mechanism (Figure 6 & Supplementary Figure S33). Most importantly, photon collection at the emission maximum of Cy5 (667 nm) revealed a 90-fold enhancement of the fluorescence signal after hybridization of ret-XCG and *comp-TCT-Cy5* to the D2 target, illustrating the exquisite sensitivity of the hybridization test with these binary probes.

CONCLUSION

In this study, our aim was to harness the potential of quenched push–pull probes to switch on a fluorescence signal through intermolecular DRET. To this end, we have developed a suitable DRET pair where the dark donor consists of a fluorene π-scaffold conjugating in a push–pull relationship, a diethylamino with a ketotriazolyl group. The acceptor was Cy5. In addition to offering far-red emission, the selected acceptor avoids detrimental cross-excitation. Once incorporated into DNAs, the fluorene derivative displayed mega-Stokes shifts (>200 nm) associated with low

quantum yields. Using DNA as a platform to control the distance, the combination of both probes allowed us to turn on the Cy5 fluorescence signal in a distance-dependent manner as expected for RET. The distance dependence of the intermolecular DRET could be exploited to accurately measure inter-chromophore distance in DNA duplexes. The performance of the X/Cy5 pair as a suitable ruler for distance measurements in DNA is currently being further explored. Combining a dark donor with mega-Stokes shifts and a bright acceptor free of cross-excitation, this DRET pair provides a fluorescence turn-on with minimal contamination. DRET probes are easy to implement and capitalize on the advantages of both MBs and binary probes. The amplification of S/N in the far-red was up to 100-fold and compares favorably with those reported for MBs (10,11,13). In order to increase it even more, the donor QY must be reduced. In the case of donor–π–acceptor dyes, this could be done by making them more sensitive to water by enhancing their push–pull character. Donors quenched by other non-radiative processes may also be considered. Screening the acceptor is an alternative and complementary approach. The S/N is directly correlated with the quantum efficiency of the acceptor, which is only 28% for Cy5. Therefore, an acceptor demonstrating a higher QY should improve the S/N. By using appropriate bandpass filters, the lack of spectral crosstalk should allow us to further optimize the collection of photons from the acceptor. As parent push–pull fluorene fluorophores exhibit a high two-photon absorption cross-section (45), the fluorene label could also be an attractive candidate for two-photon excitation in the NIR. Therefore, new opportunities for the construction of binary probes are expected for sensing applications in life sciences and detection in the far-red with minimal background fluorescence (46,47).

SUPPLEMENTARY DATA

Supplementary Data are available at NAR Online.

ACKNOWLEDGEMENTS

We thank the French Government for the PhD grants of G.B. and J.S.

FUNDING

French 'Agence Nationale de la Recherche' [PFPImaging – 18-CE09-0020-01]; Y.M. is grateful to the 'Institut Universitaire de France (IUF)'. Funding for open access charge: Agence Nationale de la Recherche; Ministère de l'Enseignement Supérieur et de la Recherche.
Conflict of interest statement. None declared.

REFERENCES

1. Medintz,I. and Hildebrandt,N. (eds.) (2013) In: *FRET – Förster Resonance Energy Transfer: From Theory to Applications*. Wiley-VCH, Weinheim, p. 791.
2. Mergny,J.-L., Boutorine,A.S., Garestier,T., Belloc,F., Rougée,M., Bulychev,N.V., Koshkin,A.A., Bourson,J., Lebedev,A.V., Valeur,B. *et al.* (1994) Fluorescence energy transfer as a probe for nucleic acid structures and sequences. *Nucleic Acids Res.*, **22**, 920–928.
3. Preus,S., Kilsa,K., Miannay,F.A., Albinsson,B. and Wilhelmsson,L.M. (2012) FRETmatrix: a general methodology for the simulation and analysis of FRET in nucleic acids. *Nucleic Acids Res.*, **41**, e18.
4. Lakowicz,J.R. (2006) In: *Principles of Fluorescence Spectroscopy. 3rd edn.*, Springer, NY, p. 954.
5. Wilhelmsson,L.M. and Tor,Y. (eds.) (2016) In: *Fluorescent Analogues of Biomolecular Building Blocks: Design and Applications*, John Wiley & Sons Inc., Hoboken, NJ, p. 448.
6. Yuan,L., Lin,W., Zheng,K. and Zhu,S. (2013) FRET-based small-molecule fluorescent probes: rational design and bioimaging applications. *Acc. Chem. Res.*, **46**, 1462–1473.
7. Cardullo,R.A., Agrawal,S., Flores,C., Zamecnik,P.C. and Wolf,D.E. (1988) Detection of nucleic acid hybridization by nonradiative fluorescence resonance energy transfer. *Proc. Natl. Acad. Sci. U.S.A.*, **85**, 8790–8794.
8. Kolpashchikov,D.M. (2010) Binary probes for nucleic acid analysis. *Chem. Rev.*, **110**, 4709–4723.
9. Martí,A.A., Jockusch,S., Stevens,N., Ju,J. and Turro,N.J. (2007) Fluorescent hybridization probes for sensitive and selective DNA and RNA detection. *Acc. Chem. Res.*, **40**, 402–409
10. Tyagi,S. and Kramer,F.R. (1996) Molecular beacons: probes that fluoresce upon hybridization. *Nat. Biotech.*, **14**, 303–308.
11. Tyagi,S., Marras,S. and Kramer,F.R. (2000) Wavelength-shifting molecular beacons. *Nat. Biotech.*, **18**, 1191–1196.
12. Li,Q., Luan,G., Guo,Q. and Liang,J. (2002) A new class of homogeneous nucleic acid probes based on specific displacement hybridization. *Nucleic Acids Res.*, **30**, e5.
13. Han,S.-X., Jia,X., Ma,J.-L. and Zhu,Q. (2013) Molecular beacons: a novel optical diagnostic tool. *Arch. Immunol. Ther. Exp.*, **61**, 139–148.
14. Santangelo,P.J. (2004) Dual FRET molecular beacons for mRNA detection in living cells. *Nucleic Acids Res.*, **32**, e57.
15. Bratu,D.P., Cha,B.-J., Mhlanga,M.M., Kramer,F.R. and Tyagi,S. (2003) Visualizing the distribution and transport of mRNAs in living cells. *Proc. Natl. Acad. Sci. U.S.A.*, **100**, 13308–13313.
16. Su,D., Oh,J., Lee,S.-C., Lim,J.M., Sahu,S., Yu,X., Kim,D. and Chang,Y.-T. (2014) Dark to light! A new strategy for large Stokes shift dyes: coupling of a dark donor with tunable high quantum yield acceptors. *Chem. Sci.*, **5**, 4812–4818.
17. Su,D., Teoh,C.L., Sahu,S., Das,R.K. and Chang,Y.-T. (2014) Live cells imaging using a turn-on FRET-based BODIPY probe for biothiols. *Biomaterials*, **35**, 6078–6085.
18. Su,D., Teoh,C.L., Kang,N.-Y., Yu,X., Sahu,S. and Chang,Y.-T. (2015) Synthesis and systematic evaluation of dark resonance energy transfer (DRET)-based library and its application in cell imaging. *Chem. Asian J.*, **10**, 581–585.
19. Şen,E., Meral,K. and Atılgan,S. (2016) From dark to light to fluorescence resonance energy transfer (FRET): polarity-sensitive aggregation-induced emission (AIE)-active tetraphenylethene-fused BODIPY dyes with a very large pseudo-Stokes shift. *Chem. - Eur. J.*, **22**, 736–745.
20. Lin,L., Lin,X., Guo,H. and Yang,F. (2017) Diphenylacrylonitrile-connected BODIPY dyes: fluorescence enhancement based on dark and AIE resonance energy transfer. *Org. Biomol. Chem.*, **15**, 6006–6013.
21. Yu,Y., Yang,B., Yuan,Y. and Zhang,H. (2019) Novel side-chain alternative copolymer combined FRET and DRET with large pseudo-Stokes shift and polarity-sensitive fluorescence behavior. *J. Mater. Chem. C*, **7**, 11285–11292.
22. Wang,X., Zhang,L., Zhuang,S., Huang,M. and Gao,Y. (2019) A novel fluorescent sensor for Sn^{4+} detection: Dark resonance energy transfer from silole to rhodamine. *Appl. Organometal. Chem.*, **114**, 590–597.
23. Armarego,W.L.F. and Chai,C.L.L. (2012) In: *Purification of Laboratory Chemicals. 7th edn.*, Butterworth-Heinemann, Oxford, p. 1024.
24. Still,W.C., Kahn,M. and Mitra,A. (1978) Rapid chromatographic technique for preparative separations with moderate resolution. *J. Org. Chem.*, **43**, 2923–2925.
25. Fulmer,G.R., Miller,A.J.M., Sherden,N.H., Gottlieb,H.E., Nudelman,A., Stoltz,B.M., Bercaw,J.E. and Goldberg,K.I. (2010) NMR chemical shifts of trace impurities: common laboratory solvents, organics, and gases in deuterated solvents relevant to the organometallic chemist. *Organometallics*, **29**, 2176–2179.

26. Sasaki,S., Niko,Y., Klymchenko,A.S. and Konishi,G.-I. (2014) Design of donor–acceptor geometry for tuning excited-state polarization: fluorescence solvatochromism of push–pull biphenyls with various torsional restrictions on their aryl–aryl bonds. *Tetrahedron*, **70**, 7551–7559.
27. Marras,S.A.E., Kramer,F.R. and Tyagi,S. (2003) Genotyping SNPs with molecular beacons. *Methods Mol. Biol.*, **212**, 111–128.
28. Breslauer,K.J. (1995) Extracting thermodynamic data from equilibrium melting curves for oligonucleotide order-disorder transitions. *Methods Enzymol.*, **259**, 221–242.
29. Brochon,J.C. (1994) Maximum entropy method of data analysis in time-resolved spectroscopy, *Methods Enzymol.*, **240**, 262–311.
30. Shaya,J., Collot,M., Bénailly,F., Mahmoud,N., Mély,Y., Michel,B.Y., Klymchenko,A.S. and Burger,A. (2017) Turn-on fluorene push-pull probes with high brightness and photostability for visualizing lipid order in biomembranes. *ACS Chem. Biol.*, **12**, 3022–3030.
31. Shaya,J., Fontaine-Vive,F., Michel,B.Y. and Burger,A. (2016) Rational design of push-pull fluorene dyes: synthesis and structure-photophysics relationship. *Chem. - Eur. J.*, **22**, 10627–10637.
32. Shaya,J., Deschamps,M.-A., Michel,B.Y. and Burger,A. (2016) Air-Stable Pd catalytic systems for sequential one-pot synthesis of challenging unsymmetrical aminoaromatics. *J. Org. Chem.*, **81**, 7566–7573.
33. Kypr,J., Kejnovska,I., Renciuk,D. and Vorlickova,M. (2009) Circular dichroism and conformational polymorphism of DNA. *Nucleic Acids Res.*, **37**, 1713–1725.
34. Hainke,S. and Seitz,O. (2009) Binaphthyl-DNA: stacking and fluorescence of a nonplanar aromatic base surrogate in DNA. *Angew. Chem. Int. Ed.*, **48**, 8250–8253.
35. Dempsey,G.T., Vaughan,J.C., Chen,K.H., Bates,M. and Zhuang,X. (2011) Evaluation of fluorophores for optimal performance in localization-based super-resolution imaging. *Nat. Methods*, **8**, 1027–1036.
36. Moreira,B.G., You,Y. and Owczarzy,R. (2015) Cy3 and Cy5 dyes attached to oligonucleotide terminus stabilize DNA duplexes: Predictive thermodynamic model. *Biophys. Chem.*, **198**, 36–44.
37. Iqbal,A., Arslan,S., Okumus,B., Wilson,T.J., Giraud,G., Norman,D.G., Ha,T. and Lilley,D.M.J. (2008) Orientation dependence in fluorescent energy transfer between Cy3 and Cy5 terminally attached to double-stranded nucleic acids. *Proc. Natl. Acad. Sci. U.S.A.*, **105**, 11176–11181.
38. Börjesson,K., Preus,S., El-Sagheer,A.H., Brown,T., Albinsson,B. and Wilhelmsson,L.M. (2009) Nucleic acid base analog FRET-pair facilitating detailed structural measurements in nucleic acid containing systems. *J. Am. Chem. Soc.*, **131**, 4288–4293.
39. Preus,S. and Wilhelmsson,L.M. (2012) Advances in quantitative FRET-based methods for studying nucleic acids. *ChemBioChem*, **13**, 1990–2001.
40. Weber,G. and Shinitzky,M. (1970) Failure of energy transfer between identical aromatic molecules on excitation at the long wave edge of the absorption spectrum. *Proc. Natl. Acad. Sci. U.S.A.*, **65**, 823–830.
41. de Rocquigny,H., El Meshri,S.E., Richert,L., Didier,P., Darlix,J.-L. and Mély,Y. (2014) Role of the nucleocapsid region in HIV-1 Gag assembly as investigated by quantitative fluorescence-based microscopy. *Virus Res.*, **193**, 78–88.
42. Becker,W. (2012) *The Bh TCSPC Handbook: Time-correlated Single Photon Counting Modules SPC-130, SPC-134, SPC-130 EM, SPC-134 EM, SPC-140, SPC-144, SPC-150, SPC-154, SPC-630, SPC-730, SPC-830; Simple-Tau Systems, SPCM Software, SPCImage Data Analysis*. Becker et Hickl.
43. Borst,J.W., Laptenok,S.P, Westphal,A.H., Kühnemuth,R., Hornen,H., Visser,N.V., Kalinin,S., Aker,J., van Hoek,A., Seidel,C.A.M. and Visser,A.J.W.G. (2008) Structural changes of yellow cameleon domains observed by quantitative FRET analysis and polarized fluorescence correlation spectroscopy. *Biophys. J.*, **95**, 5399–5411.
44. Kashida,H., Kurihara,A., Kawai,H. and Asanuma,H. (2017) Orientation-dependent FRET system reveals differences in structures and flexibilities of nicked and gapped DNA duplexes. *Nucleic Acids Res.*, **45**, e105.
45. Kucherak,O.A., Didier,P., Mély,Y. and Klymchenko,A.S. (2010) Fluorene analogues of prodan with superior fluorescence brightness and solvatochromism. *J. Phys. Chem. Lett.*, **1**, 616–620.
46. Jin,Z., Geißler,D., Qiu,X., Wegner,K.D. and Hildebrandt,N. (2015) A rapid, amplification-free, and sensitive diagnostic assay for single-step multiplexed fluorescence detection of MicroRNA. *Angew. Chem. Int. Ed.*, **54**, 10024–10029.
47. Sharma,K.K., Przybilla,F., Restle,T., Godet,J. and Mély,Y. (2016) FRET-based assay to screen inhibitors of HIV-1 reverse transcriptase and nucleocapsid protein. *Nucleic Acids Res.*, **44**, e74.